Development 139, 1276-1284 (2012) doi:10.1242/dev.072728

Differential regulation of node formation, nodal ciliogenesis and cilia positioning by *Noto* and *Foxj1*

Leonie Alten[1], Karin Schuster-Gossler[1], Anja Beckers[1], Stephanie Groos[2], Bärbel Ulmer[3], Jan Hegermann[4], Matthias Ochs[4] and Achim Gossler[1,*]

SUMMARY

The mouse transcription factor *Noto* is expressed in the node and controls node morphogenesis, formation of nodal cilia and left-right asymmetry. *Noto* acts upstream of *Foxj1*, which regulates ciliogenesis in other mouse tissues. However, the significance of *Foxj1* for the formation of cilia in the mouse node is unclear; in non-amniote species *Foxj1* is required for ciliogenesis in the structures equivalent to the node. Here, we analyzed nodes, nodal cilia and nodal flow in mouse embryos in which we replaced the *Noto*-coding sequence with that of *Foxj1*, or in embryos that were deficient for *Foxj1*. We show that *Foxj1* expressed from the *Noto* locus is functional and restores the formation of structurally normal motile cilia in the absence of *Noto*. However, *Foxj1* is not sufficient for the correct positioning of cilia on the cell surface within the plane of the nodal epithelium, and cannot restore normal node morphology. We also show that *Foxj1* is essential for ciliogenesis upstream of *Rfx3* in the node. Thus, the function of *Foxj1* in vertebrate organs of asymmetry is conserved, and *Noto* regulates node morphogenesis and the posterior localization of cilia on node cells independently of *Foxj1*.

KEY WORDS: Mouse node, Cilia, Left-right determination

INTRODUCTION

The node is a transient structure at the anterior end of the primitive streak of amniote vertebrate embryos that is essential for embryo patterning (reviewed by Camus and Tam, 1999; Viebahn, 2001). In mouse embryos, the node becomes morphologically visible around embryonic day (E) 7.5 at the distal tip of the embryo as a shallow, crescent-shaped depression on the endodermal side. At this stage, the node constitutes the posterior extreme of the forming notochord (PNC) (Blum et al., 2007), the ventral cell layer of which faces the outer curvature of the embryo with its apical side. Hereafter, we refer to the node/PNC as 'node' for simplicity. Each ventral node cell carries a monocilium that protrudes into the extracellular space on its apical surface (Sulik et al., 1994). The core of a cilium, the so-called axoneme, consists of a stereotypically arranged set of microtubules that originates at the so-called basal body, which is anchored in the cortical actin cytoskeleton. The basal body of a primary cilium is a centrosomal structure consisting of a mother centriole, which serves as the organizing center for the axonemal microtubules, and a closely attached perpendicular daughter centriole (reviewed by Nigg and Raff, 2009). Nodal cilia are motile, but in general their axonemes contain only nine peripheral doublet microtubules and lack the central microtubule pair that is characteristic for motile cilia (Feistel and Blum, 2006; Satir and Christensen, 2007). However, some nodal cilia with a central microtubule pair were also observed (Caspary et al., 2007). Monocilia in the central node rotate clockwise. This rotation, in combination with the posterior localization of the cilium on the cell surface and the posteriorly tilted rotational axis, leads to the generation of a leftward nodal flow of extra-embryonic fluid (Nonaka et al., 1998). This flow generates a symmetry-breaking signal by mechanically stimulating sensory monocilia on cells unilaterally in the periphery of the node (McGrath et al., 2003; Shiratori and Hamada, 2006) or by establishing a gradient of a secreted morphogen (Nonaka et al., 1998; Okada et al., 2005). Ultimately, this signal is translated into the asymmetry of visceral organs. Mutations that affect the formation and structure (Nonaka et al., 1998; Marszalek et al., 1999; Takeda et al., 1999; Murcia et al., 2000; Taulman et al., 2001; Huangfu et al., 2003; Huangfu and Anderson, 2005; Houde et al., 2006), sensory function (Pennekamp et al., 2002) or motility (Supp et al., 1997; Watanabe et al., 2003) of monocilia in the node disrupt the normal generation of left-right asymmetry, demonstrating their essential role in this process.

Noto is the mouse member of the Not family of homeobox genes. Not genes are expressed in the node of amniotes, or in Kupffer's vesicle in bony fish and the gastrocoel roof plate in amphibians, which represent the homologous structures to the murine node (von Dassow et al., 1993; Knezevic et al., 1995; Stein and Kessel, 1995; Talbot et al., 1995; Abdelkhalek et al., 2004; Plouhinec et al., 2004). In mouse embryos, *Noto* is required in the node and for normal notochord formation in and posterior to the lower trunk region (Abdelkhalek et al., 2004). Left-right determination in the embryo depends on *Noto* in the node, where it regulates node morphogenesis and ciliogenesis. Embryos lacking *Noto* display nodes with highly variable and irregular shapes and sizes. Cilia in *Noto* mutant nodes are short, and basal bodies are often detached from the apical cell surface. In *Noto* mutants, several genes important for cilia function or assembly are downregulated, and cilia have disorganized or incomplete

[1]Institute for Molecular Biology, Medizinische Hochschule Hannover, Carl-Neuberg-Strasse 1, D-30625 Hannover, Germany. [2]Department of Cell Biology, Medizinische Hochschule Hannover, Carl-Neuberg-Strasse 1, D-30625 Hannover, Germany. [3]University of Hohenheim, Institute of Zoology (220), Garbenstrasse 30, D-70593 Stuttgart, Germany. [4]Institute of Functional and Applied Anatomy, Medizinische Hochschule Hannover, Carl-Neuberg-Strasse 1, D-30625 Hannover, Germany.

*Author for correspondence (gossler.achim@mh-hannover.de)

Accepted 13 January 2012

axonemal microtubules (Beckers et al., 2007). Among the genes directly or indirectly regulated by *Noto* are those encoding the transcription factors *Foxj1* and *Rfx3*, which are expressed in the node and in many other tissues containing ciliated cells (Reith et al., 1994; Blatt et al., 1999; Brody et al., 2000). FOXJ1 and RFX3 regulate the expression of a number of genes important for cilia structure and function and directly activate an overlapping set of target genes (reviewed by Thomas et al., 2010). Loss of RFX3 leads to short but ultrastructurally normal nodal cilia, and causes left-right defects (Bonnafe et al., 2004). Likewise, loss of FOXJ1 causes left-right defects, although apparently normal cilia were observed in the node, whereas cilia are absent from multi-ciliated lung epithelial cells (Chen et al., 1998; Brody et al., 2000). In the absence of *Noto*, *Foxj1* and *Rfx3* are downregulated in the node. This raises several questions: which of the defects in *Noto* mutant nodes are caused by reduced *Foxj1* and *Rfx3* expression; which of these defects are direct consequences of loss of NOTO and which are mediated by an as yet unidentified factor; and what is the regulatory relationship between *Foxj1* and *Rfx3*. To address these questions, we generated mice expressing *Foxj1* instead of *Noto* and analyzed nodes and nodal cilia in these embryos and in embryos deficient for *Foxj1*. Our analyses indicate that *Rfx3* acts downstream of *Foxj1* in the node and that *Foxj1* expression is necessary for the generation of motile nodal cilia. In the absence of functional *Noto*, *Foxj1* is sufficient to restore motile cilia in the node, and *Noto* functions independently of *Foxj1* in node morphogenesis and polarized localization of cilia in the node.

MATERIALS AND METHODS

Mouse lines and genotyping

To express *Foxj1* instead of *Noto* we replaced GFP in the targeting vector used to generate the $Noto^{GFP}$ null allele (Abdelkhalek et al., 2004) by the *Foxj1* coding sequence followed by IRES2-tdtomato and a neo cassette flanked by frt sites. Gene targeting, ES cell screening and chimera production was carried out as described for the $Noto^{GFP}$ allele. The neo cassette was excised by crossing germ line chimeras to FLPe deleter mice (Rodriguez et al., 2000). The $Noto^{Foxj1}$ allele after neo excision was genotyped by PCR using the primers Foxj1Ki-Neo-F1 (AGACCGAGATAGGGTTGAGTGTTG) and Δ–neo-B (GCAACCCACACACATAAAAAGGAG); the wt and $Noto^{GFP}$ alleles were genotyped as described (Abdelkhalek et al., 2004). $Foxj1^{lacZ/+}$ mice (Brody et al., 2000) were genotyped by allele-specific PCR using primers HGT1 (TTCAAGGGCAGATGGAGAGAGG) and HGT4 (AGCCGTGGGGGTCTGTGC) resulting in a 519 bp wild-type product, and HGT1 and HGT-lacZ (CTCTTCGCTATTACGCCAGCTGG) resulting in a 416 bp product indicative of the mutant allele. All mouse work performed conformed to the regulatory standards for experimental animal work as set out by the legal authorities.

In situ hybridization

Mutant and wild-type embryos were processed in parallel under identical conditions by standard procedures (Beckers et al, 2007). Pictures were obtained as described previously (Beckers et al., 2007).

Direct video microscopy of nodal cilia

Motility of nodal cilia was analyzed as described (Schweickert et al., 2007).

Video microscopy and image analysis for nodal flow analysis

The flow of fluorescent beads (125-fold dilution of FluoSpheres, 0.5 μm, Molecular Probes in F10 culture Media, Gibco) in the cavity of the PNC/ventral node was recorded for durations of at least 60 seconds as described (Schweickert et al., 2007) at 10 frames per second (fps) and at 20× magnification using a Zeiss AxioMot2 equipped with an AxioCam HSm video camera. Trajectories were visualized using ImageJ software in combination with the MTrackJ plugin (http://www.imagescience.org/meijering/software/mtrackj/). Time-lapse movies were analyzed and transformed into trajectories by ParticleTracker (Sbalzarini and Koumoutsakos, 2005) (ImageJ; http://rsb.info.nih.gov/ij/). Trajectories were processed by a custom-made script for project-R (http://cran.r-project.org/) as described (Schweickert et al., 2007; Maisonneuve et al., 2009).

Scanning electron microscopy

Embryos were dissected in ice-cold phosphate-buffered saline (PBS) and immediately fixed in 0.1 M sodium cacodylate buffer, pH 7.4, with 3% glutaraldehyde overnight followed by washes in 0.1 M sodium cacodylate buffer, post-fixation in 2% OsO_4 in 0.1 M sodium cacodylate buffer and dehydration in a graded acetone series. Embryos were critical-point dried, mounted and sputter coated with gold. Analysis was performed using an SEM 505 microscope (Philips, Eindhoven, The Netherlands).

Transmission electron microscopy

Embryos were dissected in ice-cold PBS, immediately fixed (2.5% glutaraldehyde, 2% formaldehyde, freshly prepared from paraformaldehyde, 1.7 mM $CaCl_2$ in 0.1 M sodium cacodylate-HCl buffer, pH 7.3) overnight, washed in 0.1 M sodium cacodylate with 0.22 M sucrose, post-fixed in 1% OsO_4 in 0.1 M sodium cacodylate followed by washes in sodium maleat buffer, pH 5.2, contrasting in 2% uranylacetat in sodium maleat buffer, washes in sodium maleat buffer, dehydration in a graded ethanol series, incubation in Toluol, Toluol/Epon 1:1 and Epon, and embedding in Epon. Specimens were oriented such that sections were perpendicular to the proximo-distal axis. Polymerization was performed for 20 hours at 40°C followed by 40 hours at 60°C. Thin sections (~65 nm thick) were collected on Formvar-coated copper slot grids and stained with uranylacetate and lead citrate. Sections were selected at lower magnifications and investigated in detail using a transmission electron microscope (Tecnai 20, FEI Company, Eindhoven, The Netherlands) at an acceleration voltage of 200 kV. To exclude influences from the arbitrary section planes, sectioned cilia were observed with electron tomography at tilt angles ranging from –70° to +70° with an increment of 1°.

Immunohistochemistry, image acquisition and processing

Embryos were dissected in ice-cold PBS and fixed for 1 hour in DMSO/MeOH/H_2O_2 (4:1:1) on ice, subjected to three 5 minute washes and a 5 hour incubation in 50 mM NH_4Cl-PBS, an 8 hour incubation in 0.1% H_2O_2/TS-PBS (1% Triton X-100, 10% FCS in PBS) and three 1 hour incubations in TS-PBS. Primary antibodies (anti-ZO1: Zytomed, #226-0031; anti-γ-tubulin: Sigma, #T 5326; anti-Dishevelled 2: abcam, #ab22616) were diluted 1:500 in TS-PBS and embryos were incubated for 3-5 days then subjected to three 1 hour washes in TS-PBS. Embryos were incubated with secondary antibodies (anti-rabbit Alexa 350, #A11046; anti-mouse Alexa 488, #A21202; anti-rabbit Alexa 488, #A21206; all Invitrogen), diluted 1:100 in TS-PBS for 16-20 hours, then washed three times in TS-PBS for 1 hour per wash. All steps were carried out at 4°C. Pictures were obtained with a Leica DMI6000B microscope and HCX PL APO 63×/1.40-0.60 Oil objective. Pictures were collected as *z*-stacks with 0.1 μm (DVL2) or 0.2 μm (ZO1/ γ-tubulin) spacing. Stacks of 25 pictures were processed using the Leica LAS AF 2.3 software. Stacks were analyzed using the 3D Deconvolution tool (Method: Blind; Refractive Index: 1.518; Auto generate PSF; ten iterations) and the projection was generated using the 3D Projection tool.

qRT-PCR

Embryos were dissected in PBS and transferred into RNAlater (Ambion, #AM7020). DNA and RNA were isolated from individual age-matched embryos using TriReagent (Sigma, #T9424) according to the manufacturer's protocol. cDNAs were synthesized from RNA samples from individual genotyped embryos using the Thermoscript RT-PCR System (Invitrogen, #11146-016) according to the manufacturer's protocol. PCRs were performed with Platinum *Taq*PCRx DNA Polymerase (Invitrogen, #11509-015) according to the basic protocol with SYBR Green and ROX (Invitrogen, #12223-012) in a 25 μl reaction volume in a 7500 Fast Real-Time PCR System (Applied Biosystems) in duplicate (at least). Gene-specific primers were checked for near 100% amplification efficiency and used to amplify short fragments of *Dynlrb2* (qDynlrb2-F1,

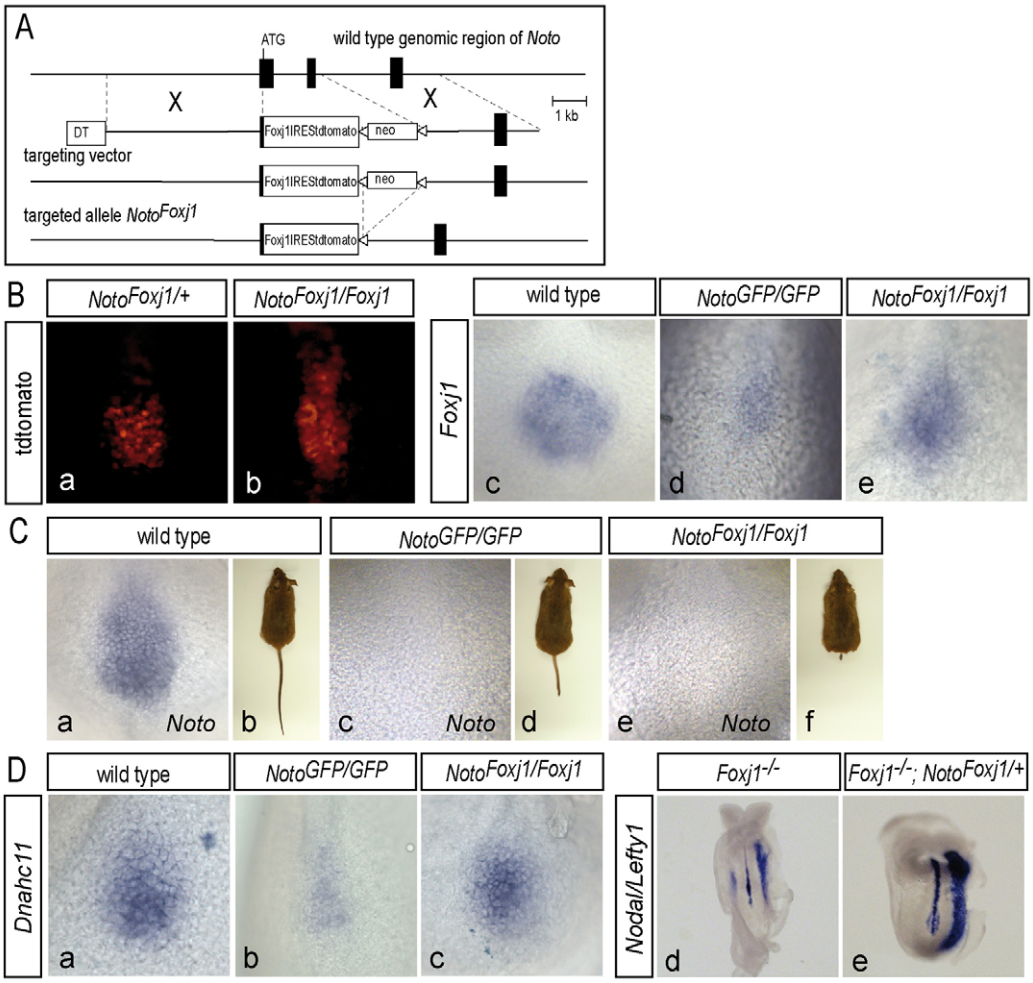

Fig. 1. Gene targeting strategy, functional validation of *Foxj1* expressed from the *Noto* locus, and external defects of *Noto*$^{Foxj1/Foxj1}$ mice. (**A**) Schematic of the genomic locus, targeting construct and targeted allele before and after FLPe mediated excision of the Neo-cassette. (**B**) Ventral views of nodes of late headfold (LHF) stage embryos. (**a**,**b**) Direct fluorescence of tdtomato. (**c-e**) Expression of *Foxj1* detected by WISH. (**C**) Expression of *Noto* in LHF stage nodes (**a**,**c**,**e**) and representative examples of adult mice (**b**,**d**,**f**); tail length of homozygous *Noto*^{Foxj1} mice is highly variable, as reported for *Noto*$^{GFP/GFP}$. (**D**) Expression of *Dnahc11*, a downstream effector of *Noto* and *Foxj1*, in LHF stage nodes (**a-c**) and ventral views of *Nodal/Lefty1* expression in 4-6 somite stage embryos (**d**,**e**). Genotypes are indicated at the top.

AGACTTGAGCCAGGAGCTGTCCCAC; qDynlrb2-B1, AGGGTTTC-CTCCACTTCTGTCATCG), *Rfx3* (qRFX3-F4, GACACCGATAGCAGT-GATGGGTGAG; qRfx3-B4, TCCAGATTTCCGGGAGATACAGCAT), *Nphp3* (qNphp3-F4, GCACAGATGTCACTGCTGCG; qNphp3-B4, TGCTGCCTATGGAATGCTCG) and *Shh* (qShh-F1, ATGAGGAAAA-CACGGGAGCAGAC; qShh-B1, AGATGGCCAAGGCATTTAAC-TTGTC). Ct-values were translated into fold change of expression levels using the ΔΔCt-method (Livak and Schmittgen, 2001). *Shh*, which is expressed in the node and in cells along the anterior midline and expression levels of which appeared to be unaffected in *Noto* or *Foxj1* mutants by whole-mount RNA in situ hybridization (WISH), served as reference gene. Mutant probes were compared with wild-type probes and the average relative wild-type expression was defined as 1. For *Rfx3*, *Nphp3* and *Shh*, a second independent PCR was performed, confirming the obtained results (data not shown).

RESULTS

Generation and characterization of *Noto*$^{Foxj1/Foxj1}$ mice

We generated a mouse that expresses functional FOXJ1 protein in the node in the absence of NOTO protein by knocking in the *Foxj1* open reading frame (followed by an internal ribosome entry site and the red fluorescent marker tdtomato) into the endogenous start codon of *Noto*. This deleted most of *Noto* exon 1, intron 1 and exon 2, and disrupted *Noto* in a similar manner to the *Noto*^{GFP} null allele that we described previously (Fig. 1A) (Abdelkhalek et al., 2004). Heterozygous mice carrying this allele (*Noto*$^{Foxj1/+}$) were phenotypically normal (data not shown). Heterozygous E7.5-8 embryos expressed *Nodal* and tektin 2 (*Tekt2*), markers for crown and pit cells, respectively, indistinguishably from wild-type embryos (data not shown), and expressed tdtomato specifically in the node, recapitulating endogenous *Noto* expression in wild-type embryos (Fig. 1Ba,b). As expected, homozygous *Noto*^{Foxj1} embryos (n=4) did not express *Noto* (Fig. 1Ce). Homozygous knock-in mice displayed shortened and kinky tails (Fig. 1Cf) that resembled the previously described *Noto*-null phenotype (Abdelkhalek et al., 2004), probably as a result of the lack of *Noto* function in the nascent notochord at later stages of development, when *Noto*, but not *Foxj1*, is expressed in wild-type embryos. In homozygous *Noto*^{Foxj1} E7.5-8 embryos (n=5), *Foxj1* mRNA was readily detected, in contrast to *Noto*-null mutants (n=5; Fig. 1Bc-e). The axonemal dynein *Dnahc11* is severely downregulated in homozygous *Noto*^{GFP} mutants (n=4; Fig. 1Db) (Beckers et al., 2007) and is a known FOXJ1 target in cells of the respiratory epithelium (Chen et al., 1998). Transgenic expression of *Foxj1* restored expression of *Dnahc11* in homozygous *Noto*^{Foxj1} embryos (n=4) at E7.5-8 (Fig. 1Dc). *Foxj1* mutant embryos (n=5) display abnormal expression of laterality genes (for example, see Fig. 1Dd). One copy of transgenic *Foxj1* expressed from the *Noto*^{Foxj1} allele restored the normal left-sided expression of *Nodal* and *Lefty1* in 4-6 somite stage embryos (n=6) lacking endogenous FOXJ1 (Fig. 1De). Collectively, these data indicate that *Foxj1* expressed from the *Noto* locus is functional and sufficient to drive expression of FOXJ1 targets in the node.

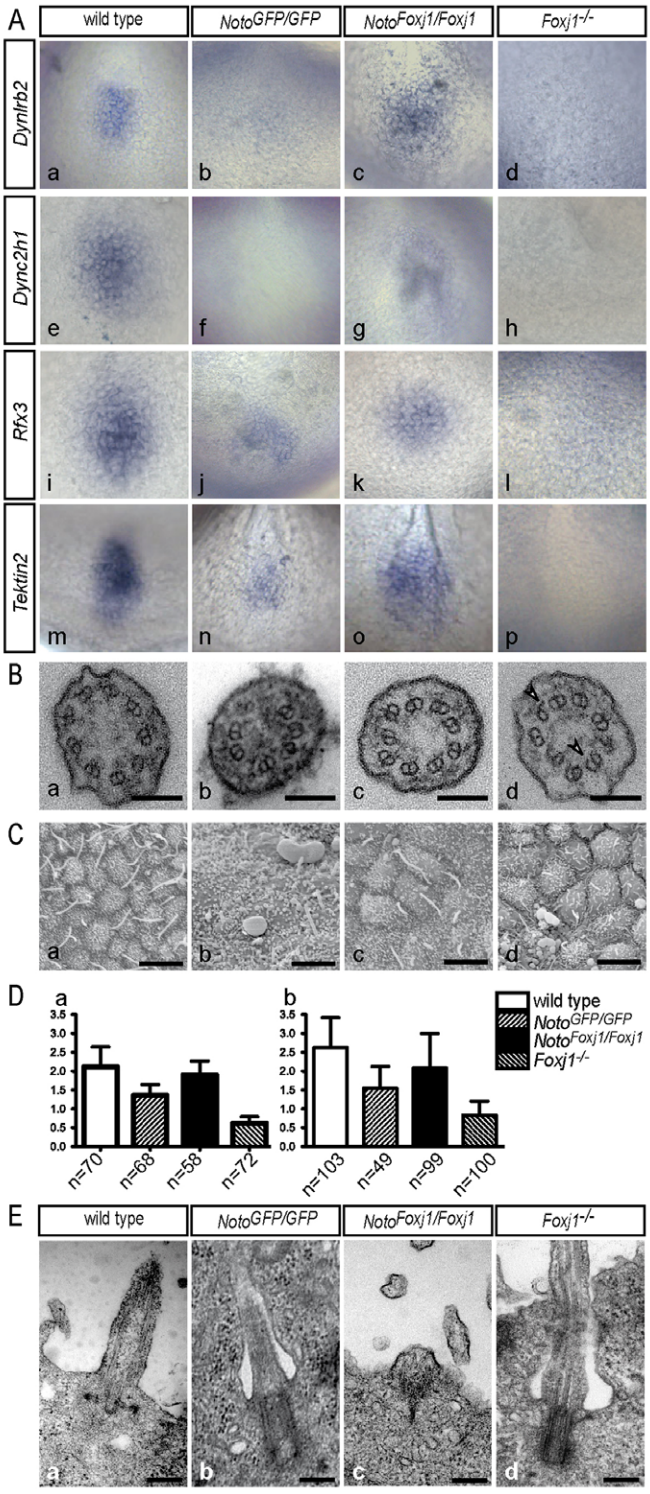

Fig. 2. Restored expression of *Noto* and *Foxj1* downstream effectors and partial rescue of cilia structure in *Noto*$^{Foxj1/Foxj1}$ embryos. (**A**) Ventral views of LHF stage embryos after WISH with probes as indicated to the left. At least four embryos per genotype and probe were used; representative examples are shown. (**B**) Transmission electron micrographs of nodal cilia of LHF stage embryos. Arrowheads in d point to disrupted or incomplete microtubules in *Foxj1*$^{-/-}$ mutants, which were also found in *Noto*$^{GFP/GFP}$ mutants. Scale bars: 100 nm. (**C**) Scanning electron micrographs of node cells of LHF stage embryos showing short cilia in *Foxj1*$^{-/-}$ and *Noto*$^{GFP/GFP}$ and restored cilia length in *Noto*^{Foxj1} mutants. Scale bars: 4 μm. (**D**) Length of nodal cilia in the indicated genotypes at the mid (**a**) and late (**b**) head fold stage. Error bars indicate s.d. $P<0.0001$. (**E**) Transmission electron micrographs of basal bodies in the node of LHF embryos. Scale bars: 200 nm. Genotypes are indicated at the top. Images (Bb and Eb) are reproduced with permission from Beckers et al. (Beckers et al., 2007).

Noto regulates expression of cilia-associated genes through *Foxj1*

We continued to analyze the consequences of *Foxj1* expression on ciliogenesis in the node, node morphology and gene expression in the absence of NOTO. Because node morphology and cilia length in the node are stage dependent (Sulik et al., 1994; Bonnafe et al., 2004), embryos were staged according to Downs and Davies (Downs and Davies, 1993) and, if not indicated otherwise, all comparative analyses were done using age-matched embryos from different litters at the late head fold stage or at a slightly earlier stage we refer to as mid head fold stage (for examples, see supplementary material Fig. S1). The loss of *Noto* function led to reduced expression of several cilia-associated genes. For example, mRNA levels of *Dynlrb2*, which encodes a cytoplasmic dynein light chain; *Dync2h1*, which encodes the heavy chain of the cytoplasmic dynein-2 retrograde motor and is a component of retrograde intraflagellar transport (Huangfu and Anderson, 2005); *Rfx3*, a transcription factor required for normal cilia growth (Bonnafe et al., 2004); and *Tekt2*, a member of a family of microtubule-stabilizing proteins (Amos, 2008) were severely reduced or not detected in *Noto*$^{GFP/GFP}$ mutants ($n\geq4$) by in situ hybridization (Beckers et al., 2007) (Fig. 2Ab,f,j,n). In homozygous *Noto*^{Foxj1} embryos, transcript levels of these genes were restored ($n\geq4$), although it appeared that full wild-type levels might not be reached (Fig. 2Ac,g,k,o). mRNA quantification by qRT-PCR (exemplarily carried out for *Dynlrb2* and *Rfx3* on independent RNA prepared from at least five embryos per genotype; Fig. 3) confirmed the severe reduction in *Noto*$^{GFP/GFP}$ mutants and revealed an upregulation to almost wild-type levels in *Noto*$^{Foxj1/Foxj1}$.

Foxj1 restores ciliogenesis and cilia motility in the absence of *Noto*

The restored expression of genes important for ciliogenesis in homozygous *Noto*^{Foxj1} nodes suggested that defective microtubule structure, shortening and immotility of cilia that were found in nodes lacking *Noto* (Beckers et al., 2007) might be rescued by the knock-in of *Foxj1* into *Noto*. In sections from six *Noto*$^{Foxj1/Foxj1}$ embryos, we observed 15 cilia, five of which could be evaluated unequivocally for the structure of axonemal microtubules by transmission electron microscopy and showed no microtubule defects (Fig. 2Bc), in contrast to the disrupted structure of axonemal microtubules in *Noto*$^{GFP/GFP}$ mutants that was described previously (Fig. 2Bb) (Beckers et al., 2007). Consistent with a previous report (Bonnafe et al., 2004), cilia length in wild-type nodes increased from the mid to late head fold stage (n=70 and 103 cilia, three and four embryos, respectively; Fig. 2Ca,D). At both stages, cilia length was significantly reduced in *Noto*$^{GFP/GFP}$ mutants (n=68 and 49, four and eight embryos, respectively; Fig. 2Cb,D), and partially restored in homozygous *Noto*^{Foxj1} embryos (n=58 and 99, three and five embryos, respectively; Fig. 2Cc,D).

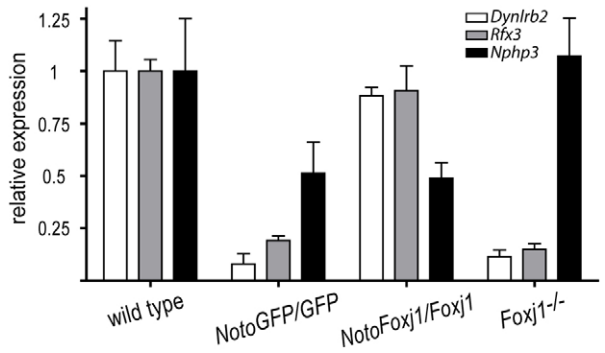

Fig. 3. *Foxj1*-dependent regulation of *Dynlrb2* and *Rfx3*, but *Foxj1*-independent regulation of *Nphp3* downstream of *Noto*. Quantitative RT-PCR analysis of *Dynlrb2*, *Rfx3* and *Nphp3* in wild-type (n=7), $Noto^{GFP/GFP}$ (n=6), $Noto^{Foxj1/Foxj1}$ (n=5) and $Foxj1^{-/-}$ (n=6) LHF embryos. Bars show relative expression levels compared with wild type; error bars indicate s.d. P<0.0001.

Nodal cilia in wild-type embryos (n=7) rotate clockwise (supplementary material Movie 1), whereas in homozygous $Noto^{GFP}$ embryos (n=3) nodal cilia are essentially immotile (Beckers et al., 2007). Nodal cilia in homozygous $Noto^{Foxj1}$ embryos (n=4) regained clockwise rotational motility (supplementary material Movie 2), indicating that *Foxj1* expression in the node is sufficient to generate motile nodal cilia in the absence of NOTO.

Foxj1 is an important regulator of ciliogenesis and cilia function in the murine node

Our finding that *Foxj1* is sufficient to restore cilia structure and motility in the *Noto*-deficient node suggests that *Foxj1* is also necessary for nodal ciliogenesis. This, however, is not consistent with previous scanning electron microscopic data that did not reveal obvious defects in nodal cilia in *Foxj1*-deficient embryos (Brody et al., 2000). To investigate this discrepancy, we analyzed expression of the above-mentioned cilia-associated genes as well as structure, length and motility of cilia in $Foxj1^{-/-}$ mutant embryos, carrying the previously analyzed $Foxj1^{-}$ allele (Brody et al., 2000). Transcripts of *Dynlrb2*, *Dync2h1*, *Rfx3* and *Tekt2* were not detected in *Foxj1*-null mutant nodes (n≥4) by in situ hybridization (Fig. 2Ad,h,l,p), and for *Dynlrb2* and *Rfx3* severe downregulation was confirmed by quantitative PCR of cDNAs from individual embryos (n=6; Fig. 3). This indicates that expression of genes important for ciliogenesis requires *Foxj1* in the node and suggests that cilia formation and function might be abnormal. In sections from six $Foxj1^{-/-}$ embryos, we could unequivocally evaluate 14 transverse sections of cilia for the structure of axonemal microtubules by transmission electron microscopy. Four out of these showed obvious defects in the structure and arrangement of axonemal microtubules (Fig. 2Bd). The difficulty of obtaining more sections of cilia might, in part, be explained by the severe reduction in the length of $Foxj1^{-/-}$ mutant cilia that we observed in scanning electron micrographs. Cilia length was reduced to about one-third in both mid and late head fold stage embryos (n=72 and 100, four and five embryos, respectively; Fig. 2Cd,D), and was more pronounced than in $Noto^{GFP/GFP}$ mutants (Fig. 2Cb,D). In addition, cilia analyzed in $Foxj1^{-/-}$ mutants (n=4) by videomicroscopy were completely immotile (supplementary material Movie 3).

Motile cilia in $Noto^{Foxj1/Foxj1}$ mutant nodes are not sufficient to generate a leftward nodal flow and establish correct left-right asymmetry

Despite the restored expression of ciliary components and wild type-like rotational motility of cilia, homozygous $Noto^{Foxj1}$ embryos displayed abnormal expression of laterality genes. In wild-type embryos, *Nodal* and *Lefty1* are expressed in the left lateral plate mesoderm and along the midline at the 4-6 somite stage (Fig. 4Aa). In homozygous $Noto^{Foxj1}$ embryos (n=7), these expression patterns were randomized. *Nodal/Lefty1* expression was detected unilaterally (on either the left or the right), was symmetrically present or absent, or was expressed at different levels on both sides (for an example, see Fig. 4Ac), resembling the defective expression of laterality genes we previously described for $Noto^{GFP/GFP}$ mutants (Beckers et al., 2007) (Fig. 4Ab). One potential explanation could be that, despite rotational movement of cilia, no normal nodal flow is established in $Noto^{Foxj1/Foxj1}$ embryos. To test this directly we observed the movement of fluorescent beads in the nodes of 2-4 somite-stage embryos by videomicroscopy. As a qualitative measure of flow, the mean resultant length of particle trails (Rayleigh's test of uniformity) was calculated from each time-lapse movie and was expressed as the dimension-less number rho (ρ). A ρ-value of 1 corresponds to movement of all beads in the same direction and ρ=0 corresponds to random movement. In wild-type embryos (n=6), fluorescent beads moved to the left side of the node (Fig. 4Ba,e, supplementary material Movie 4) with a ρ of 0.62. Consistent with immotile cilia, there was essentially no directional movement of beads in $Noto^{GFP/GFP}$ (ρ=0.08; Fig. 4Bb,f, supplementary material Movie 5) and $Foxj1^{-/-}$ (ρ=0.09; Fig. 4Bd,h, supplementary material Movie 7) mutant embryos (n=8, respectively). Directional movement in $Noto^{Foxj1/Foxj1}$ nodes (ρ=0.21; n=5; Fig. 4Bc,g, supplementary material Movie 6) was slightly higher than in $Noto^{GFP/GFP}$ and $Foxj1^{-/-}$, but clearly reduced compared with wild type. This supports the idea that abnormal nodal flow underlies the laterality defects in these embryos despite restored cilia length and motility.

Noto is required for proper node morphogenesis

Left-right defects can be caused by an irregular shape of the node (Lee et al., 2010). Because $Noto^{GFP/GFP}$ mutant embryos have irregular nodes of variable size and show abnormal expression patterns of genes delineating the node (e.g. Beckers et al., 2007) (Fig. 4Cf,n,Db,f,j), we analyzed node morphology in homozygous $Noto^{Foxj1}$ embryos by scanning electron microscopy (n=8) and marker gene expression. These analyses showed that nodes in homozygous $Noto^{Foxj1}$ embryos had variable shapes and sizes similar to nodes in $Noto^{GFP/GFP}$ embryos (compare Fig. 4Cf,n with 4Cg,o). This was also reflected by abnormal expression domains of marker genes for node cells. The area of *Nphp3* (n=4) and *Shh* (n=6) expression was variable and compressed, and the width and shape of the crown cell region delineated by expression of *Dand5* (n=3) was no longer horseshoe-shaped but was narrow and irregular (Fig. 4Dc,g,k). By contrast, in $Foxj1^{-/-}$ mutant embryos (n=9), which retain *Noto* expression (supplementary material Fig. S2), the shape of the node (Fig. 4Ch,p), as well as the expression patterns of *Nphp3* (n=5), *Shh* (n=4) and *Dand5* (n=5) (Fig. 4Dd,h,l) were essentially normal, although the nodes appeared somewhat smaller in some $Foxj1^{-/-}$ mutant embryos.

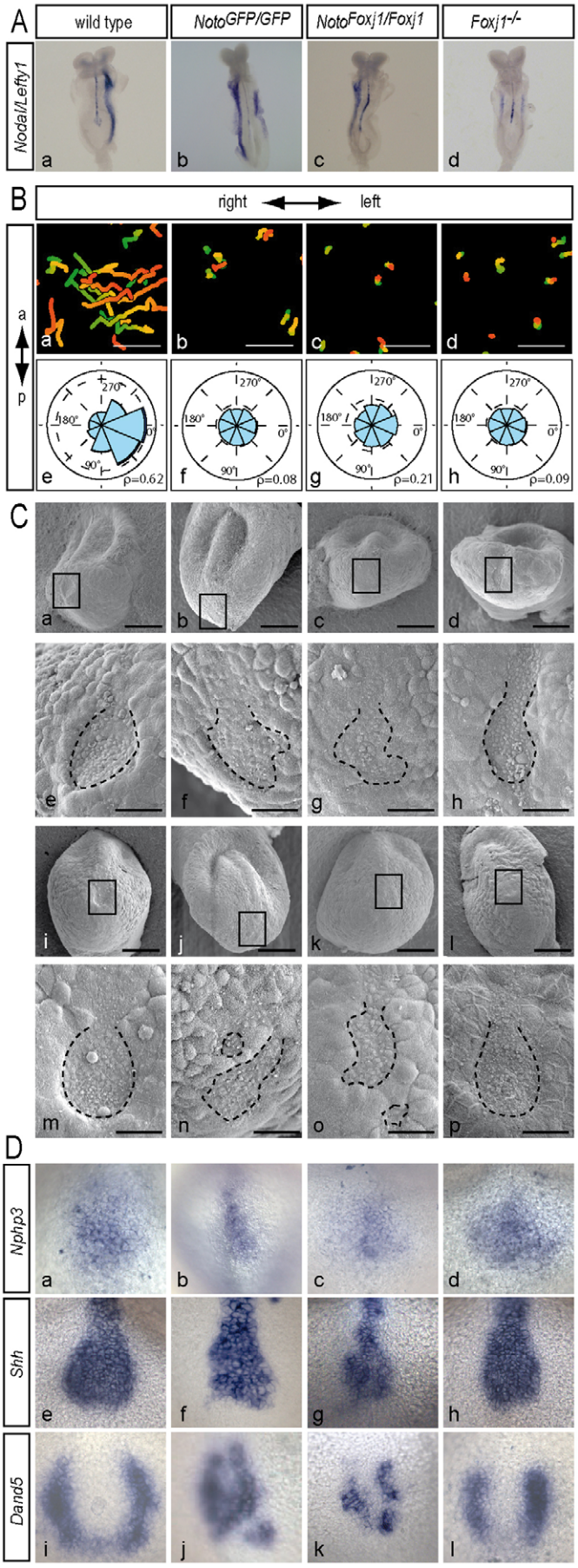

Fig. 4. Laterality and nodal flow defects, and abnormal node/PNC structure in *Noto*$^{Foxj1/Foxj1}$ embryos. (**A**) Representative examples ($n \geq 5$) of 4-6 somite stage embryos hybridized with probes for *Nodal* and *Lefty1*. (**B**) Analysis of nodal flows in embryos with 2-4 somites. (**a-d**) Trajectories of fluorescent beads in the node region displayed as gradient timed trails of 2 seconds length. Scale bars: 25 μm. The green color indicates the start, red the final position. (**e-h**) Frequency distributions of trajectory directionalities in wild type (six movies, 739 particles, angle 21.7°, ρ: 0.62), *Noto*$^{GFP/GFP}$ (eight movies, 470 particles, angle: 65.54°, ρ: 0.08), *Noto*$^{Foxj1/Foxj1}$ (five movies, 384 particles, angle: 19.18°, ρ: 0.21) and *Foxj1*$^{-/-}$ (eight movies, 462 particles, angle: 71.09°, ρ: 0.09). The cones reflect the directionality frequencies for eight given ranges of angles. Dashed circles mark the highest frequencies in percent (33.83% for wild-type, 15.53% for *Noto*$^{GFP/GFP}$, 19.27% for *Noto*$^{Foxj1/Foxj1}$ and 15.37% for *Foxj1*$^{-/-}$ embryos). Solid circles mark 40% boundaries. 0° marks the left side of the node. (**C**) Representative scanning electron micrographs of LHF stage embryos (**a-d**,**i-l**) and enlargements of the respective node regions (**e-h**,**m-p**). Scale bars: in a-d,i-l, 100 μm; in e-h,m-p, 40 μm. Boxes in a-d, and i-l indicate the enlarged node regions shown in e-h and m-p. Dashed lines in e-h, and m-p indicate areas with ciliated cells. Images shown in j and n are reproduced with permission from Beckers et al. (Beckers et al., 2007). (**D**) Altered expression patterns of *Nphp3*, *Shh* and *Dand5* in LHF stage embryos. Probes and genotypes are indicated to the left and at the top, respectively.

Defective polarized localization of nodal cilia in *Noto*$^{GFP/GFP}$, *Noto*$^{Foxj1/Foxj1}$ and *Foxj1*$^{-/-}$ mutant embryos

Effective nodal flow requires the polarized location of cilia in the plane of node cells towards the posterior end (Nonaka et al., 2005; Antic et al., 2010). To investigate whether mislocalization of cilia could also contribute to defective left-right patterning, we analyzed the position of cilia on node cells in scanning electron micrographs of embryos of the various genotypes. In wild-type nodes, in >75% of the cells (n=78/103 in four embryos) cilia were anchored at the posterior pole of the cell (Fig. 5Aa,Ba). By contrast, ~50% of the cilia in *Noto*$^{GFP/GFP}$ (n=27/49 in eight embryos), *Noto*$^{Foxj1/Foxj1}$ (n=49/99 in five embryos) and *Foxj1*$^{-/-}$ mutants (n=50/100 in five embryos) emerged at a central position, the others at roughly equal rates anterior, posterior, left or right to the central position (Fig. 5Ab-d,Ba, supplementary material Table S1). To confirm independently that the position of cilia is randomized in mutant embryos, we stained embryos with antibodies against γ-tubulin, which marks centriolar structures including the basal bodies, and ZO1, which outlines the cell borders (Fig. 5Ae-h). Consistent with our analysis of scanning electron micrographs in >75% of wild-type node cells (n=194/251 in six embryos), basal bodies were located at the posterior pole of the cell, whereas only 13% of the cilia in *Noto*$^{GFP/GFP}$ (n=19/147 in eight embryos), 14% in *Noto*$^{Foxj1/Foxj1}$ (n=25/182 in seven embryos) and 15% in *Foxj1*$^{-/-}$ mutants (n=24/155 in seven embryos) were located at this position (Fig. 5Bb, supplementary material Table S1). Thus, the abnormal positioning of cilia in the nodes of *Noto*$^{Foxj1/Foxj1}$ and *Foxj1*$^{-/-}$ embryos might prevent the generation of an effective leftward flow and contribute to defective left-right patterning.

DISCUSSION

In *Noto* mutant embryos, node morphogenesis and nodal ciliogenesis are disrupted. Here, we have shown that expression of *Foxj1* from the *Noto* locus is sufficient to restore the motility of

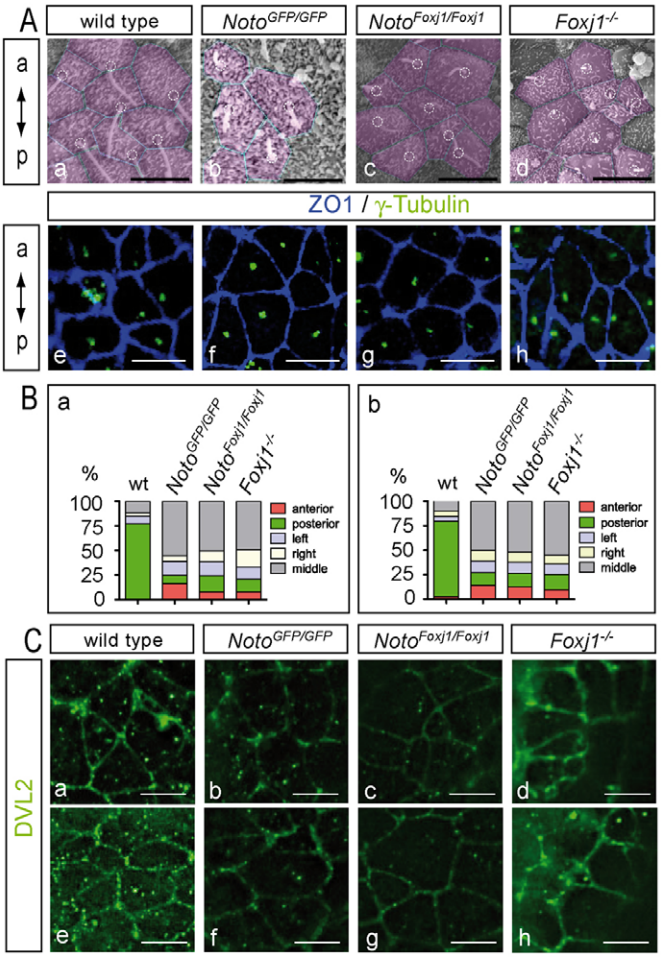

Fig. 5. Abnormal positioning of nodal cilia in *Noto*$^{Foxj/Foxj1}$ embryos. (**A**) (**a-d**) Representative examples of scanning electron micrographs of node regions of late headfold stage embryos used for evaluation of cilia position. Dashed lines mark cell borders. Dashed circles indicate the bases of cilia. (**e-h**) Representative examples of LHF stage embryos stained by immunofluorescence with antibodies marking basal bodies (γ-tubulin, green) and tight junctions (ZO1, blue) used for evaluation of cilia position. Genotypes are indicated at the top, orientation of embryos is shown at the left. (**B**) Quantification of cilia position analyzed in electron micrographs (**a**) and in fluorescent micrographs (**b**) after antibody staining. (**C**) Pictures of ciliated cells in the node region of late headfold stage embryos stained with an antibody against DVL2 showing reduced DVL2 levels at the apical edge of the lateral membrane in *Noto*$^{GFP/GFP}$ and *Noto*$^{Foxj1/Foxj1}$ mutants compared with wild type and *Foxj1*$^{-/-}$. Scale bars: 4 μm. Genotypes are indicated at the top.

cilia and the transcription of genes important for ciliogenesis in mutants lacking *Noto* function. The rescue of gene expression and cilia structure in *Noto*$^{Foxj1/Foxj1}$ embryos is consistent with cilia defects in *Foxj1*$^{-/-}$ mutant embryos and indicates that in mouse embryos *Noto* regulates essential aspects of nodal ciliogenesis through *Foxj1*. In addition, we have provided evidence that *Foxj1* is indispensable for the formation of functional motile cilia in the murine node. This finding is in line with *Foxj1* function in *Xenopus* and zebrafish embryos. In these species, *Foxj1* is required for the formation of cilia in the gastrocoel roof plate and Kupffer's vesicle, respectively (Stubbs et al., 2008), which represent structures equivalent to the node.

We detected *Rfx3* mRNA in the node only in the presence of *Foxj1* expression (Fig. 2Ai-l). Thus, in node cells there appears to be a clear epistatic relationship between *Foxj1* and *Rfx3*, with *Foxj1* acting upstream of *Rfx3*. This differs from cultured multiciliated mouse ependymal cells, in which RFX3 regulated *Foxj1* expression (El Zein et al., 2009), and from mouse floorplate cells, in which expression of *Rfx3* was unaffected by the loss of *Foxj1* (Cruz et al., 2010). Thus, the regulatory relationship between these two transcription factors that govern ciliogenesis appears to differ between the node and other tissues. It is noteworthy that ectopic expression of *Foxj1* in neural progenitors converted short primary cilia into long cilia, but in *Foxj1* mutant floorplate cells cilia length was unaffected, which was attributed to redundant functions of *Rfx3* and *Foxj1* (Cruz et al., 2010). In cultured mouse ependymal cells, loss of *Rfx3* function led to reduced growth of motile cilia and affected expression of genes involved in cilia assembly and motility (El Zein et al., 2009). Similarly, in the mouse node, *Rfx3* mutants have short but ultrastructurally normal cilia (Bonnafe et al., 2004) raising the possibility that reduced or absent *Rfx3* expression in both *Noto* and *Foxj1* mutants might underlie the 'short cilia' phenotype and defective motility in both mutants. *Noto*$^{GFP/GFP}$ mutants expressed *Foxj1* at a low, but still detectable, level (Fig. 1Bd). Genes that were severely downregulated but still detected in *Noto*$^{GFP/GFP}$ mutants (Fig. 2Aj,n) were not detected in *Foxj1*$^{-/-}$ mutants (Fig. 2Al,p), and cilia length was less reduced in *Noto*$^{GFP/GFP}$ than in *Foxj1*$^{-/-}$ mutant nodes (Fig. 2D). Altogether, these defects in *Noto*$^{GFP/GFP}$ mutants appear to be slightly milder than those of *Foxj1*$^{-/-}$ mutants, which might be due to residual *Foxj1* activity in *Noto*$^{GFP/GFP}$ mutants, and further supports the notion that *Noto* regulates crucial aspects of ciliogenesis through *Foxj1* and *Rfx3*. By contrast, *Foxj1* expression does not restore node morphogenesis in the absence of NOTO and *Foxj1*$^{-/-}$ embryos exhibit normal node morphology. These findings indicate that *Noto* regulates pivotal aspects of node morphogenesis independently of *Foxj1*, and suggest that the abnormal shape of nodes in *Noto*$^{Foxj1/Foxj1}$ embryos, rather than undetected irregularities in the motion of *Noto*$^{Foxj1/Foxj1}$ nodal cilia, contributes to the left-right defects. However, we cannot exclude the possibility that abnormal transcript levels of *Foxj1* expressed from the *Noto* locus contribute to some of the remaining defects in *Noto*$^{Foxj1/Foxj1}$ embryos.

Mutants lacking *Noto* or *Foxj1* function showed randomized positions of cilia on the surface of node cells. This could indicate that both genes function together to localize cilia at the posterior cell pole. We cannot rule out this possibility, but the random positioning of cilia might also arise for different reasons in the different genotypes. In *Foxj1* mutant airway epithelial cells, no cilia form, apical actin and ezrin localization is disrupted, and basal bodies are not anchored at the cell cortex (Huang et al., 2003; Gomperts et al., 2004; Pan et al., 2007). In the node of *Foxj1*$^{-/-}$ mutants, two out of seven detected centriolar structures (daughter centrioles or basal bodies without an emerging cilium in the plane of section), were located abnormally deep in the cytoplasm, and we found sections of a cilium emerging from a basal body in a deep indentation of the plasma membrane (Fig. 2Ed). Centriolar structures that were located abnormally deep in the cytoplasm and cilia emerging from such deep basal bodies were also observed in *Noto*$^{GFP/GFP}$ mutant embryos (Fig. 2Eb) (Beckers et al., 2007) but not in sections from *Noto*$^{Foxj1/Foxj1}$ mutant nodes (Fig. 2Ec), although we cannot rule out the possibility that such cilia or basal bodies exist but were not observed. These observations raise the possibility that basal bodies are not correctly localized at the cell

cortex in *Foxj1*$^{-/-}$ mutant node cells, similar to airway epithelial cells, which might contribute to the abnormal cilia positioning in nodes lacking *Foxj1*. In *Noto*$^{Foxj1/Foxj1}$ nodes, cilia might not be correctly localized for a different reason. In these mutants, expression of known *Foxj1* targets but not *Nphp3* (nephrocystin 3; nephronophthisis 3 – Mouse Genome Informatics) was restored (Fig. 3). NPHP3 protein interacts with inversin, a component of the planar cell polarity (PCP) signaling pathway, and is required for convergent extension cell movements in *Xenopus* embryos, suggesting a role in establishing planar cell polarity (Bergmann et al., 2008). Loss of *Nphp3* function in mice disrupts normal left-right asymmetry (Olbrich et al., 2003; Bergmann et al., 2008). Thus, the reduced expression of *Nphp3* in *Noto*$^{GFP/GFP}$ mutants raises the possibility that defective PCP signaling contributes to left-right defects by abnormal cilia positioning in the nodes of these embryos. However, it is unclear whether the observed reduction of *Nphp3* levels in *Noto*$^{GFP/GFP}$ and *Noto*$^{Foxj1/Foxj1}$ mutants is sufficient to cause PCP defects, because no such defects were described in heterozygous *Nphp3* mutants (Bergmann et al., 2008). Although microarray analyses did not detect transcriptional downregulation of known PCP pathway components in *Noto*$^{GFP/GFP}$ mutants (L.A., A.B. and A.G., unpublished observation), we tried to detect potential alterations in the distribution of known PCP proteins in *Noto* mutant node cells. Although commercially available VANGL1 and PRICKLE2 antibodies did not work reliably in our hands, DVL2 protein was consistently reduced at the apical membrane of node cells in *Noto*$^{GFP/GFP}$ and *Noto*$^{Foxj1/Foxj1}$ mutants (n=5 each) compared with wild-type (n=6) and *Foxj1*$^{-/-}$mutant (n=6) nodes (Fig. 5C). However, Dvl genes function redundantly in the mouse node (Hashimoto et al., 2010), and it is unclear whether the localization and/or amount of other DVL proteins is also affected. Nonetheless, as basal bodies appear to be correctly attached at the apical cortex in *Noto*$^{Foxj1/Foxj1}$ mutants, but fail to localize posteriorly, our data suggest that posterior localization of cilia is controlled by *Noto* in a *Foxj1*-independent manner.

In summary, our analysis has distinguished processes in the mouse node directly regulated by *Noto* from processes requiring *Foxj1* and *Rfx3* function, and has established the regulatory relationship between *Foxj1* and *Rfx3*. *Foxj1* is indispensable for functional nodal cilia, and acts upstream of *Rfx3*. *Noto* regulates nodal ciliogenesis by means of *Foxj1*, but *Noto* is required for node morphogenesis independently of *Foxj1*, and establishes the posterior localization of cilia potentially by affecting planar cell polarity.

Acknowledgements

We thank Dr R. Y. Tsien (La Jolla, CA, USA) for the tdtomato cDNA; Dr S. Brody (St Louis, MO, USA) for *Foxj1* mutant mice; Thomas Thumberger for the ImageJ macro 'Cellgridder' and tools for the nodal flow analysis; Dr U. Lehmann-Mühlenhoff for support with the quantitative PCR; and Drs M. Blum and M. Stauber for discussion and critical comments on the manuscript.

Funding

This work was supported by institutional funding for the Research Core Unit for Electron Microscopy at Hannover Medical School (to M.O.), by a PhD fellowship from the Landesgraduiertenförderung Baden-Württemberg (to B.U.), by funding from the Deutsche Forschungsgemeinschaft (DFG) [GO 449/6-3 to A.G.] and by the DFG funded Cluster of Excellence REBIRTH (to A.G.). Deposited in PMC for immediate release.

Competing interests statement

The authors declare no competing financial interests.

Supplementary material

Supplementary material available online at
http://dev.biologists.org/lookup/suppl/doi:10.1242/dev.072728/-/DC1

References

Abdelkhalek, H. B., Beckers, A., Schuster-Gossler, K., Pavlova, M. N., Burkhardt, H., Lickert, H., Rossant, J., Reinhardt, R., Schalkwyk, L. C., Muller, I. et al. (2004). The mouse homeobox gene Not is required for caudal notochord development and affected by the truncate mutation. *Genes Dev.* **18**, 1725-1736.

Amos, L. A. (2008). The tektin family of microtubule-stabilizing proteins. *Genome Biol.* **9**, 229.

Antic, D., Stubbs, J. L., Suyama, K., Kintner, C., Scott, M. P. and Axelrod, J. D. (2010). Planar cell polarity enables posterior localization of nodal cilia and left-right axis determination during mouse and *Xenopus* embryogenesis. *PLoS ONE* **5**, e8999.

Beckers, A., Alten, L., Viebahn, C., Andre, P. and Gossler, A. (2007). The mouse homeobox gene Noto regulates node morphogenesis, notochordal ciliogenesis, and left right patterning. *Proc. Natl. Acad. Sci. USA* **104**, 15765-15770.

Bergmann, C., Fliegauf, M., Brüchle, N. O., Frank, V., Olbrich, H., Kirschner, J., Schermer, B., Schmedding, I., Kispert, A., Kränzlin, B. et al. (2008). Loss of nephrocystin-3 function can cause embryonic lethality, Meckel-Gruber-like syndrome, situs inversus, and renal-hepatic-pancreatic dysplasia. *Am. J. Hum. Genet.* **82**, 959-970.

Blatt, E. N., Yan, X. H., Wuerffel, M. K., Hamilos, D. L. and Brody, S. L. (1999). Forkhead transcription factor HFH-4 expression is temporally related to ciliogenesis. *Am. J. Respir. Cell Mol. Biol.* **21**, 168-176.

Blum, M., Andre, P., Muders, K., Schweickert, A., Fischer, A., Bitzer, E., Bogusch, S., Beyer, T., van Straaten, H. W. and Viebahn, C. (2007). Ciliation and gene expression distinguish between node and posterior notochord in the mammalian embryo. *Differentiation* **75**, 133-146.

Bonnafe, E., Touka, M., AitLounis, A., Baas, D., Barras, E., Ucla, C., Moreau, A., Flamant, F., Dubruille, R., Couble, P. et al. (2004). The transcription factor RFX3 directs nodal cilium development and left-right asymmetry specification. *Mol. Cell. Biol.* **24**, 4417-4427.

Brody, S. L., Yan, X. H., Wuerffel, M. K., Song, S. K. and Shapiro, S. D. (2000). Ciliogenesis and left-right axis defects in forkhead factor HFH-4-null mice. *Am. J. Respir. Cell Mol. Biol.* **23**, 45-51.

Camus, A. and Tam, P. P. (1999). The organizer of the gastrulating mouse embryo. *Curr. Top. Dev. Biol.* **45**, 117-153.

Caspary, T., Larkins, C. E. and Anderson, K. V. (2007). The graded response to Sonic Hedgehog depends on cilia architecture. *Dev. Cell* **12**, 767-778.

Chen, J., Knowles, H. J., Hebert, J. L. and Hackett, B. P. (1998). Mutation of the mouse hepatocyte nuclear factor/forkhead homologue 4 gene results in an absence of cilia and random left-right asymmetry. *J. Clin. Invest.* **102**, 1077-1082.

Cruz, C., Ribes, V., Kutejova, E., Cayuso, J., Lawson, V., Norris, D., Stevens, J., Davey, M., Blight, K., Bangs, F. et al. (2010). Foxj1 regulates floor plate cilia architecture and modifies the response of cells to sonic hedgehog signalling. *Development* **137**, 4271-4282.

Downs, K. M. and Davies, T. (1993). Staging of gastrulating mouse embryos by morphological landmarks in the dissecting microscope. *Development* **118**, 1255-1266.

El Zein, L., Ait-Lounis, A., Morlé, L., Thomas, J., Chhin, B., Spassky, N., Reith, W. and Durand, B. (2009). RFX3 governs growth and beating efficiency of motile cilia in mouse and controls the expression of genes involved in human ciliopathies. *J. Cell Sci.* **122**, 3180-3189.

Feistel, K. and Blum, M. (2006). Three types of cilia including a novel 9+4 axoneme on the notochordal plate of the rabbit embryo. *Dev. Dyn.* **235**, 3348-3358.

Gomperts, B. N., Gong-Cooper, X. and Hackett, B. P. (2004). Foxj1 regulates basal body anchoring to the cytoskeleton of ciliated pulmonary epithelial cells. *J. Cell. Sci.* **117**, 1329-1337.

Hashimoto, M., Shinohara, K., Wang, J., Ikeuchi, S., Yoshiba, S., Meno, C., Nonaka, S., Takada, S., Hatta, K., Wynshaw-Boris, A. et al. (2010). Planar polarization of node cells determines the rotational axis of node cilia. *Nat. Cell Biol.* **12**, 170-177.

Houde, C., Dickinson, R. J., Houtzager, V. M., Cullum, R., Montpetit, R., Metzler, M., Simpson, E. M., Roy, S., Hayden, M. R., Hoodless, P. A. et al. (2006). Hippi is essential for node cilia assembly and Sonic hedgehog signaling. *Dev. Biol.* **300**, 523-533.

Huang, T., You, Y., Spoor, M. S., Richer, E. J., Kudva, V. V., Paige, R. C., Seiler, M. P., Liebler, J. M., Zabner, J., Plopper, C. G. et al. (2003). Foxj1 is required for apical localization of ezrin in airway epithelial cells. *J. Cell. Sci.* **116**, 4935-4945.

Huangfu, D. and Anderson, K. V. (2005). Cilia and Hedgehog responsiveness in the mouse. *Proc. Natl. Acad. Sci. USA* **102**, 11325-11330.

Huangfu, D., Liu, A., Rakeman, A. S., Murcia, N. S., Niswander, L. and Anderson, K. V. (2003). Hedgehog signalling in the mouse requires intraflagellar transport proteins. *Nature* **426**, 83-87.

Knezevic, V., Ranson, M. and Mackem, S. (1995). The organizer-associated chick homeobox gene, Gnot1, is expressed before gastrulation and regulated synergistically by activin and retinoic acid. *Dev. Biol.* **171**, 458-470.

Lee, J. D., Migeotte, I. and Anderson, K. V. (2010). Left-right patterning in the mouse requires Epb4.1l5-dependent morphogenesis of the node and midline. *Dev. Biol.* **346**, 237-246.
Livak, K. J. and Schmittgen, T. D. (2001). Analysis of relative gene expression data using real-time quantitative PCR and the 2(-Delta Delta C(T)) method. *Methods* **25**, 402-408.
Maisonneuve, C., Guilleret, I., Vick, P., Weber, T., Andre, P., Beyer, T., Blum, M. and Constam, D. B. (2009). Bicaudal C, a novel regulator of Dvl signaling abutting RNA-processing bodies, controls cilia orientation and leftward flow. *Development* **136**, 3019-3030.
Marszalek, J. R., Ruiz-Lozano, P., Roberts, E., Chien, K. R. and Goldstein, L. S. (1999). Situs inversus and embryonic ciliary morphogenesis defects in mouse mutants lacking the KIF3A subunit of kinesin-II. *Proc. Natl. Acad. Sci. USA* **96**, 5043-5048.
McGrath, J., Somlo, S., Makova, S., Tian, X. and Brueckner, M. (2003). Two populations of node monocilia initiate left-right asymmetry in the mouse. *Cell* **114**, 61-73.
Murcia, N. S., Richards, W. G., Yoder, B. K., Mucenski, M. L., Dunlap, J. R. and Woychik, R. P. (2000). The Oak Ridge Polycystic Kidney (orpk) disease gene is required for left-right axis determination. *Development* **127**, 2347-2355.
Nigg, E. A. and Raff, J. W. (2009). Centrioles, centrosomes, and cilia in health and disease. *Cell* **139**, 663-678.
Nonaka, S., Tanaka, Y., Okada, Y., Takeda, S., Harada, A., Kanai, Y., Kido, M. and Hirokawa, N. (1998). Randomization of left-right asymmetry due to loss of nodal cilia generating leftward flow of extraembryonic fluid in mice lacking KIF3B motor protein. *Cell* **95**, 829-837.
Nonaka, S., Yoshiba, S., Watanabe, D., Ikeuchi, S., Goto, T., Marshall, W. F. and Hamada, H. (2005). De novo formation of left-right asymmetry by posterior tilt of nodal cilia. *PLoS Biol.* **3**, e268.
Okada, Y., Takeda, S., Tanaka, Y., Belmonte, J. C. and Hirokawa, N. (2005). Mechanism of nodal flow: a conserved symmetry breaking event in left-right axis determination. *Cell* **121**, 633-644.
Olbrich, H., Fliegauf, M., Hoefele, J., Kispert, A., Otto, E., Volz, A., Wolf, M. T., Sasmaz, G., Trauer, U., Reinhardt, R. et al. (2003). Mutations in a novel gene, NPHP3, cause adolescent nephronophthisis, tapeto-retinal degeneration and hepatic fibrosis. *Nat. Genet.* **34**, 455-459.
Pan, J., You, Y., Huang, T. and Brody, S. L. (2007). RhoA-mediated apical actin enrichment is required for ciliogenesis and promoted by Foxj1. *J. Cell Sci.* **120**, 1868-1876.
Pennekamp, P., Karcher, C., Fischer, A., Schweickert, A., Skryabin, B., Horst, J., Blum, M. and Dworniczak, B. (2002). The ion channel polycystin-2 is required for left-right axis determination in mice. *Curr. Biol.* **12**, 938-943.
Plouhinec, J. L., Granier, C., Le Mentec, C., Lawson, K. A., Saberan-Djoneidi, D., Aghion, J., Shi, D. L., Collignon, J. and Mazan, S. (2004). Identification of the mammalian Not gene via a phylogenomic approach. *Gene Expr. Patterns* **5**, 11-22.
Reith, W., Ucla, C., Barras, E., Gaud, A., Durand, B., Herrero-Sanchez, C., Kobr, M. and Mach, B. (1994). RFX1, a transactivator of hepatitis B virus enhancer I, belongs to a novel family of homodimeric and heterodimeric DNA-binding proteins. *Mol. Cell. Biol.* **14**, 1230-1244.
Rodriguez, C. I., Buchholz, F., Galloway, J., Sequerra, R., Kasper, J., Ayala, R., Stewart, A. F. and Dymecki, S. M. (2000). High-efficiency deleter mice show that FLPe is an alternative to Cre-loxP. *Nat. Genet.* **25**, 139-140.
Satir, P. and Christensen, S. T. (2007). Overview of structure and function of mammalian cilia. *Annu. Rev. Physiol.* **69**, 377-400.
Sbalzarini, I. F. and Koumoutsakos, P. (2005). Feature point tracking and trajectory analysis for video imaging in cell biology. *J. Struct. Biol.* **151**, 182-195.
Schweickert, A., Weber, T., Beyer, T., Vick, P., Bogusch, S., Feistel, K. and Blum, M. (2007). Cilia-driven leftward flow determines laterality in *Xenopus*. *Curr. Biol.* **17**, 60-66.
Shiratori, H. and Hamada, H. (2006). The left-right axis in the mouse: from origin to morphology. *Development* **133**, 2095-2104.
Stein, S. and Kessel, M. (1995). A homeobox gene involved in node, notochord and neural plate formation of chick embryos. *Mech. Dev.* **49**, 37-48.
Stubbs, J. L., Oishi, I., Izpisua Belmonte, J. C. and Kintner, C. (2008). The forkhead protein Foxj1 specifies node-like cilia in *Xenopus* and zebrafish embryos. *Nat. Genet.* **40**, 1454-1460.
Sulik, K., Dehart, D. B., Inagaki, T., Carson, J. L., Vrablic, T., Gesteland, K. and Schoenwolf, G. C. (1994). Morphogenesis of the murine node and notochordal plate. *Dev. Dyn.* **201**, 260-278.
Supp, D. M., Witte, D. P., Potter, S. S. and Brueckner, M. (1997). Mutation of an axonemal dynein affects left-right asymmetry in inversus viscerum mice. *Nature* **389**, 963-966.
Takeda, S., Yonekawa, Y., Tanaka, Y., Okada, Y., Nonaka, S. and Hirokawa, N. (1999). Left-right asymmetry and kinesin superfamily protein KIF3A: new insights in determination of laterality and mesoderm induction by kif3A–/– mice analysis. *J. Cell Biol.* **145**, 825-836.
Talbot, W. S., Trevarrow, B., Halpern, M. E., Melby, A. E., Farr, G., Postlethwait, J. H., Jowett, T., Kimmel, C. B. and Kimelman, D. (1995). A homeobox gene essential for zebrafish notochord development. *Nature* **378**, 150-157.
Taulman, P. D., Haycraft, C. J., Balkovetz, D. F. and Yoder, B. K. (2001). Polaris, a protein involved in left-right axis patterning, localizes to basal bodies and cilia. *Mol. Biol. Cell* **12**, 589-599.
Thomas, J., Morlé, L., Soulavie, F., Laurençon, A., Sagnol, S. and Durand, B. (2010). Transcriptional control of genes involved in ciliogenesis: a first step in making cilia. *Biol. Cell* **102**, 499-513.
Viebahn, C. (2001). Hensen's node. *Genesis* **29**, 96-103.
von Dassow, G., Schmidt, J. E. and Kimelman, D. (1993). Induction of the Xenopus organizer: expression and regulation of Xnot, a novel FGF and activin-regulated homeo box gene. *Genes Dev.* **7**, 355-366.
Watanabe, D., Saijoh, Y., Nonaka, S., Sasaki, G., Ikawa, Y., Yokoyama, T. and Hamada, H. (2003). The left-right determinant Inversin is a component of node monocilia and other 9+0 cilia. *Development* **130**, 1725-1734.

Table S1. Quantification of cilia position

Method used to determine cilia position		Wild type	*Noto*$^{GFP/GFP}$	*Noto*$^{Foxj1/Foxj1}$	*Foxj1*$^{-/-}$
Electron microscopy	Total number of cilia in *n* embryos	103 in four embryos	49 in eight embryos	99 in five embryos	100 in five embryos
	Anterior	0 (0.0%)	8 (16.3%)	8 (8.0%)	8 (8.0%)
	Posterior	78 (77.2%)	4 (8.2%)	13 (13.0%)	16 (16.0%)
	Middle	12 (11.9%)	27 (55.1%)	49 (49.0%)	50 (50.0%)
	Left	8 (7.9%)	7 (14.3%)	12 (12.0%)	14 (14.0%)
	Right	3 (3.0%)	3 (6.1%)	18 (18.0%)	11 (11.0%)
Immuno-fluorescence staining	Total number of cilia in *n* embryos	251 in six embryos	147 in eight embryos	182 in seven embryos	156 in seven embryos
	Anterior	6 (2.4%)	21 (14.3%)	23 (12.6%)	15 (9.6%)
	Posterior	194 (77.3%)	19 (12.9%)	25 (13.7%)	24 (15.4%)
	Middle	25 (10.0%)	74 (50.3%)	94 (51.6%)	86 (55.1%)
	Left	12 (4.8%)	17 (11.6%)	21 (11.5%)	17 (10.9%)
	Right	14 (5.6%)	16 (10.9%)	19 (10.4%)	14 (9.0%)